Numerical Assessment Concerning a Focused Microwave Diagnostic Method for Medical Applications

Salvatore Caorsi, *Member, IEEE*, Andrea Massa, and Matteo Pastorino, *Senior Member, IEEE*

***Abstract*—The possibility of focused microwave imaging in medical applications is investigated in this paper by means of a numerical assessment based on the forward scattering solution. As a text case, a human abdomen is considered and different electromagnetic sources operating at the working frequencies $f = 433$ MHz and $f = 2.45$ GHz are used. Many numerical investigations are performed in order to define the optimal dimensions of the reduced investigation domain. To quantitatively evaluate the effects of the reduction of the original investigation domain on the inversion data, suitable relative errors are defined. Once the reduced domain is defined, preliminary reconstructions are performed, aiming to evaluate the imaging capabilities of a global optimization technique when a focused approach is used for tomographic applications. Finally, some considerations are drawn and future developments of the proposed technique are indicated.**

***Index Terms*—Genetic algorithms, inverse problems, medical diagnosis, microwave imaging.**

I. Introduction

WHEN microwave imaging was proposed as a noninvasive technique in medical applications, the potential advantages of this technology seemed to allow for great and rapid developments [1], [2]. In the context of medical diagnostics, microwave imaging was indicated as the future leading technique for microwave dosimetry, and a lot of possible applications were proposed, including diagnostic tools integrating active and passive methodologies.

Although a lot of work has been done by several research groups over the last years [3]–[18], microwave imaging is not yet competitive, as compared with other more consolidated diagnostic techniques. The reason is ultimately related to the mechanism of interaction between microwaves and biological tissues. In general, microwave-imaging methods try to infer information concerning biological tissues starting by measurements performed outside the body under test. In active imaging, an incident field is used to interrogate the body. The problem one has to handle is, in general, an inverse scattering problem, which is strongly nonlinear and ill posed [19]. In general, multiple scattering cannot be neglected and methods similar to those usually applied in X-ray computed tomography (CT) and based on ray propagation (sometimes with certain compensations) have been found to produce rather limited results. Although diffraction tomography approaches have been proven to be able to generate quantitative images of biological bodies in a quasi-real time, they are usually based on weakly scattering approximations (e.g., Born or Rytov approximations) and are unable to accurately reconstruct strongly contrasted bodies [20]. Moreover, the expected spatial resolution is limited by the wavelength of the incident wave.

Recently, accurate reconstructions have been obtained by using inverse scattering methods in the spatial domain. These approaches are usually based on discretization of the integral equations of the inverse scattering problem. A number of techniques (most of them iterative) have been applied in order to solve the discretized equations, in several cases by recasting the problem as an optimization process in which a functional is defined and minimized. These methods are able to deal with highly contrasted bodies. In addition, it has been demonstrated that the achievable resolution is not limited by the wavelength of the incident field, but discretizations finer than those dictated by the Raleigh criterion can be used.

Although these integral-equation approaches are rather efficient, they are usually too time consuming to allow the use of discretizations suitable for producing images detailed enough to be useful in medical applications. Moreover, the risk of reaching nonglobal (local) minima is particularly critical in the medical field, as they correspond to "artefacts" in the final image.

In the authors' opinion, the possibility of focused imaging should be further evaluated, in which only a part of the biological body is subjected to the investigation. Moreover, with reduced investigation domains, it would be possible to concentrate the computational resources for this region and to apply a global optimization approach [21], which is able, in principle, to reach the global minimum.

To this end, the aim of this paper is twofold. First of all, we report a numerical investigation concerning the possibility of reducing the domain inside a model of a human abdomen. The investigation area is defined according to the results of direct scattering simulations in which parts of the body are neglected. The possibility of reducing the investigation domain is strongly related to the power penetration inside the body and, consequently, on the focused incident field. Different illuminations will be considered in the analysis.

It should be mentioned that a focused approach to microwave imaging was previously studied by Caorsi *et al.* [12]. That approach was "exact" in the sense that the Green's function for

Manuscript received November 29, 1999; revised May 3, 2000.

S. Caorsi and A. Massa are with the Department of Electronics, University of Pavia, 27100 Pavia, Italy (e-mail: caorsi@dibe.unige.it; massa@dibe.unige.it).

M. Pastorino is with the Department of Biophysical and Electronic Engineering, University of Genoa, 16145 Genoa, Italy (e-mail: pastorino@dibe.unige.it).

Publisher Item Identifier S 0018-9480(00)09533-8.

the inhomogeneous structure represented by the biological body was numerically calculated (off-line). Although the results obtained by inverting the data by using a pseudoinversion algorithm with a reduced domain were quite interesting, the need for the computation of the Green's function requires an accurate model of the biological body under test. Due to the wide range of geometric/dielectric changes among different patients, large errors can be expected unless the numerical Green's function is computed for any specific case (the approach seems to be more suitable, for example, in industrial applications, where the "unperturbed" objects to be inspected is usually completely known). In this paper, we aim to assess how a domain reduction will affect the possible reconstruction of a limited domain. Roughly speaking, the scattering by the neglected part of the body can be considered as noise in the measurement data.

The second objective of this paper is the application of a global optimization technique based on a genetic algorithm (GA) [22], [23] to produce an image of the reduced investigation domain. Although GAs are usually very time consuming when implemented on serial computers, they exhibit some interesting features that can be summarized as follows.

1) They allow, in principle, to reach the global minimum (avoiding "artefacts" in the final image of the biological body).
2) They allow the straightforward introduction into the model of *a priori* information. A lot of *a priori* information is usually available, particularly in the medical field, but, in general it is very difficult to take into account this information using deterministic techniques. *A priori* information may concern the range of values of the dielectric parameters or even the boundaries between different tissues. Such boundaries may be known from different diagnostic techniques. This represents an example of the possibility (offered by methods in which the *a priori* information can be directly inserted into the model) of using different diagnostic methodologies in a complementary way
3) GAs allow a straightforward parallelization and a rather simple hybridization with deterministic minimization procedures.

Finally, it should be mentioned that, besides the issues related to data inversion and image formation, the development of medical microwave-imaging approaches is also limited both by theoretical aspects [19] (e.g., uniqueness issues and nonradiating currents) and experimental difficulties connected to the design and realization of efficient and fast illumination and measurement systems. These two last aspects are not considered here, and the reader is referred to the wide literature on this subject [6], [9], [24].

II. Reduced Investigation Domain

The first question we point out is essentially the following: when imaging a biological system, is it possible to focus our attention only on a limited part of that body, neglecting the remaining part? In tomographic applications, two-dimensional models are usually assumed. In this context, as a test case, we consider the simplified model of a human abdomen reported in

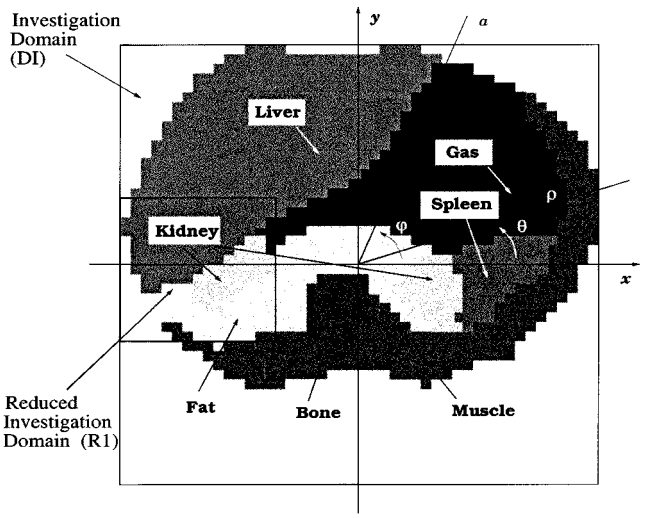

Fig. 1. Schematized human abdomen. Reduced investigation and observation domains.

Fig. 1. In microwave imaging, the body is illuminated by an incident field (or a set of incident fields) and the scattered field is collected in a suitable observation domain. TM illumination conditions are used. The unknown dielectric parameters of the body are then retrieved by inverting the mathematical equations of the resulting inverse-scattering problem. The recently proposed imaging methods (which are developed in the spatial domain) require a discretization of the cross section of the biological body. Due to multiple scattering, the whole cross section should be discretized. Whatever method is used, a very fine spatial resolution can be expected only for organs of small cross section (e.g., arms or legs). In cases similar to the one considered here (i.e., human abdomen), the discretization of the whole section would make the problem almost intractable, at least if a stochastic optimization approach is to be used (without a parallel implementation).

Let us consider now a reduced square investigation domain, denoted by R1 and located inside the original cross section (denoted by DI). The original cross section is partitioned into $N = 46 \times 46$ square subdomains of side $1 = 0.5$ cm. The above discretization is sufficient to obtain an accurate forward solution by using the method of moments [25], [26]. Moreover, the following illuminating sources are considered:

1) plane wave impinging with an incident angle φ whose incident electric field is given by $\mathbf{E}_{\text{inc}}(x, y) = E_0 \exp\{+jk\rho\}\mathbf{z}$, k being the wavenumber in the external medium (free space), and $\mathbf{z}$ being the unit vector of the z-axis;
2) infinite line source located at point (a, φ) (polar coordinates), with $a = 16.5$ cm (fixed):

$$\mathbf{E}_{\text{inc}}(x, y) = -I \frac{k^2}{4\omega\varepsilon_0} H_0^{(2)}(kr)\mathbf{z}$$

$H_0^{(2)}$ being the Hankel function of second kind and zero order, r is the distance between point (a, φ) and point (x, y), ε_0 is the free-space dielectric constant, and ω is the angular frequency;

3) focusing source (in the transverse plane), which is modeled (by using an equation similar to Silver's equation [27] for directive antennas) as

$$\mathbf{E}_{\rm inc}(x, y) = -I \frac{k^2}{4\omega\varepsilon_0} H_0^{(2)}(kr) D(\varphi')\mathbf{z}$$

where $D(\varphi') = \sqrt{\sin^n(\varphi')}$ if $0 \le \varphi' \le \pi$ and $D(\varphi') = 0$ elsewhere, being n an integer number and φ' the polar angle in a coordinate system centered in (a, φ) and having the y-axis passing through the origin ($\rho = 0$).

For case 2), we assume I such that a radiated power for unit length of $P = 1$ mW/m is generated by the infinite source. Using the asymptotic expansions for Bessel functions [27], I is obtained by $I = \sqrt{8P/\eta k}$, where η is the intrinsic impedance of the free space.

The same value of I is used for case 3). For the first simulations, a frequency of 433 MHz is assumed. The cross-sectional DI is modeled by a scattering potential

$$\tau(x, y) = \varepsilon_0 \left[\varepsilon_r(x, y) - j \frac{\sigma(x, y)}{\omega\varepsilon_0} - 1\right]$$

where $\varepsilon_r(x, y)$ and $\sigma(x, y)$ are the relative dielectric permittivity and electric conductivity of the biological tissues (Table I) [28]. Finally, the observation domain (DM) is a circle of radius $b = 16.4$ cm and the location of the generic measurement point is (b, θ). Due to the TM illumination, only the z-component of the fields are considered.

The side of R1 is firstly evaluated. Since the contribution to the scattered electric field of each subdomain is essentially a function of the polarization current in the same subdomain (assumed to be constant and denoted by $J_m = \tau_m E^m_{\rm tot}$, where $\tau_m = \tau(x_m, y_m)$, $E^m_{\rm tot} = E_{\rm tot}(x_m, y_m)$, and (x_m, y_m) is the center of the mth subdomain), this quantity is considered. In particular, Fig. 2 gives the percentage of subdomains for which, after solving the forward problem involving the whole cross section DI, we obtained $|J_m| \ge J_{\rm th}$, where $J_{\rm th}$ is a threshold value. Fig. 2 reports this percentage for the various illumination conditions and for any possible value of φ, $0 \le \varphi \le 2\pi$ (angular step: $\pi/12$). This figure gives some indications concerning the possible dimensions of R1. As expected, the plane wave illumination represents the worst case, whereas moderately focused sources are more suitable for this application. For low angles, due to the crude discretized model of the human abdomen, the presence of a nonrealistic interface between the internal air region and surrounding one results in low percentage values (the focused source illuminates a limited part of the body). However, excluding this limited angular range, the various plots exhibit rather regular behaviors. This means that approximately the same values for the side of R1 can be the choice for any φ.

The question is now the following: what is an acceptable threshold? The choice of the threshold is related to the errors on the scattered electric field in the observation domain. In the following, according to the previous consideration, we assume a fixed value $\varphi = \pi$ and evaluate in detail the case of $(J_{\rm th}/J_{\rm max}) = 30\%$, where $J_{\rm max}$ in the maximum value of $|J_m|$ inside DI. According to Fig. 2(d), a reasonable choice is d (side of R1) $= 7.5$ cm. Fig. 3 gives the behavior of the incident and scattered electric fields (amplitudes) inside the whole cross-sectional DI. Moreover, Fig. 4 shows the behavior of the same fields along (a) vertical and (b) horizontal axes. In Fig. 5, the plots of the incident, scattered, and total electric fields (amplitudes) in the observation domain are also given. Figs. 3–5 are related to the various illumination conditions defined at points (a)–(c). It should be noted that since a reduced investigation domain is used, Fig. 5 can provide useful information concerning the angular location of the measurement points on the observation domain. In particular, receivers with $\theta \approx \varphi$ should be avoided due to the blinding effect of the source, whereas insufficient information is present for the largest values of $(\theta - \pi)$. However, it should be noted that, for source (c) with $n = 2$ and $n = 3$, a large range of θ values exist for which $|E_{\rm inc}(x, y)|$ is rather small [see Fig. 5(a)].

TABLE I
SCATTERING POTENTIALS OF THE VARIOUS TISSUES OF THE SCHEMATIZED HUMAN ABDOMEN FOR THE TWO FREQUENCIES $f = 433$ MHz AND $f = 2.45$ GHz

	$f = 433$ MHz		$f = 2.45$ GHz	
	$\frac{Re\{\tau\}}{\varepsilon_0}$	$\frac{Im\{\tau\}}{\varepsilon_0}$	$\frac{Re\{\tau\}}{\varepsilon_0}$	$\frac{Im\{\tau\}}{\varepsilon_0}$
Liver	46.5	-35.72	41.5	-14.82
Muscle	52.0	-59.36	46.0	-16.21
Bone	4.60	-3.23	4.50	-1.13
Kidney	53.0	-48.98	47.0	-13.38
Spleen	74.0	-61.44	65.0	-16.87
Fat	4.60	-3.23	4.50	-1.13

Let us consider now the investigation domain R1 only, neglecting the other part of the cross section (denoted by $\mathrm{R2} = \mathrm{DI} - \mathrm{R1}$). Fig. 6 provides a comparison between the scattered and total electric field computed considering the whole cross-sectional DI and considering $R1$ only. For small angles around $\theta = \pi$, there is a good agreement between the total field (i.e., the measurements) in the two cases. This consideration, as well as the previous ones concerning the illuminating sources, can be used to define the angular region where it will be convenient to locate the receivers.

In order to better evaluate the weights of the various contributions to the scattering, the scattered electric field at point (b, θ) can be expressed as the sum of four terms

$$E_{\rm scatt}(b, \theta) = \sum_{i=1}^{2} \sum_{j=1}^{2} \{L_{ij}(b, \theta)\} \tag{1}$$

$$L_{ij}(b, \theta) = \int_{Ri} \tau_i(x', y') E_{{\rm tot}_{ij}}(x', y') \cdot G(b, \theta/x', y')\, dx'\, dy' \tag{2}$$

where $\tau_i(x, y)$ denotes the scattering potential in the ith region, $E_{{\rm tot}_{ij}}(x, y)$ denotes the total electric field in the same region due to the polarization current density in the jth region, and G is the two-dimensional Green's function for free space. Assuming $\tau_2(x, y) = 0$ is equivalent to neglect $L_{12}(b, \theta)$, $L_{21}(b, \theta)$, and $L_{22}(b, \theta)$. Denoting by $\alpha(\theta) = |L_{12}(b, \theta)|$ and $\beta(\theta) = |L_{21}(b, \theta) + L_{22}(b, \theta)|$, Fig. 7 shows the behavior of $\alpha(\theta)$ and $\beta(\theta)$ for any θ and for the different sources considered. Roughly speaking, $\alpha(\theta)$ refers to the partial scattering contribution of

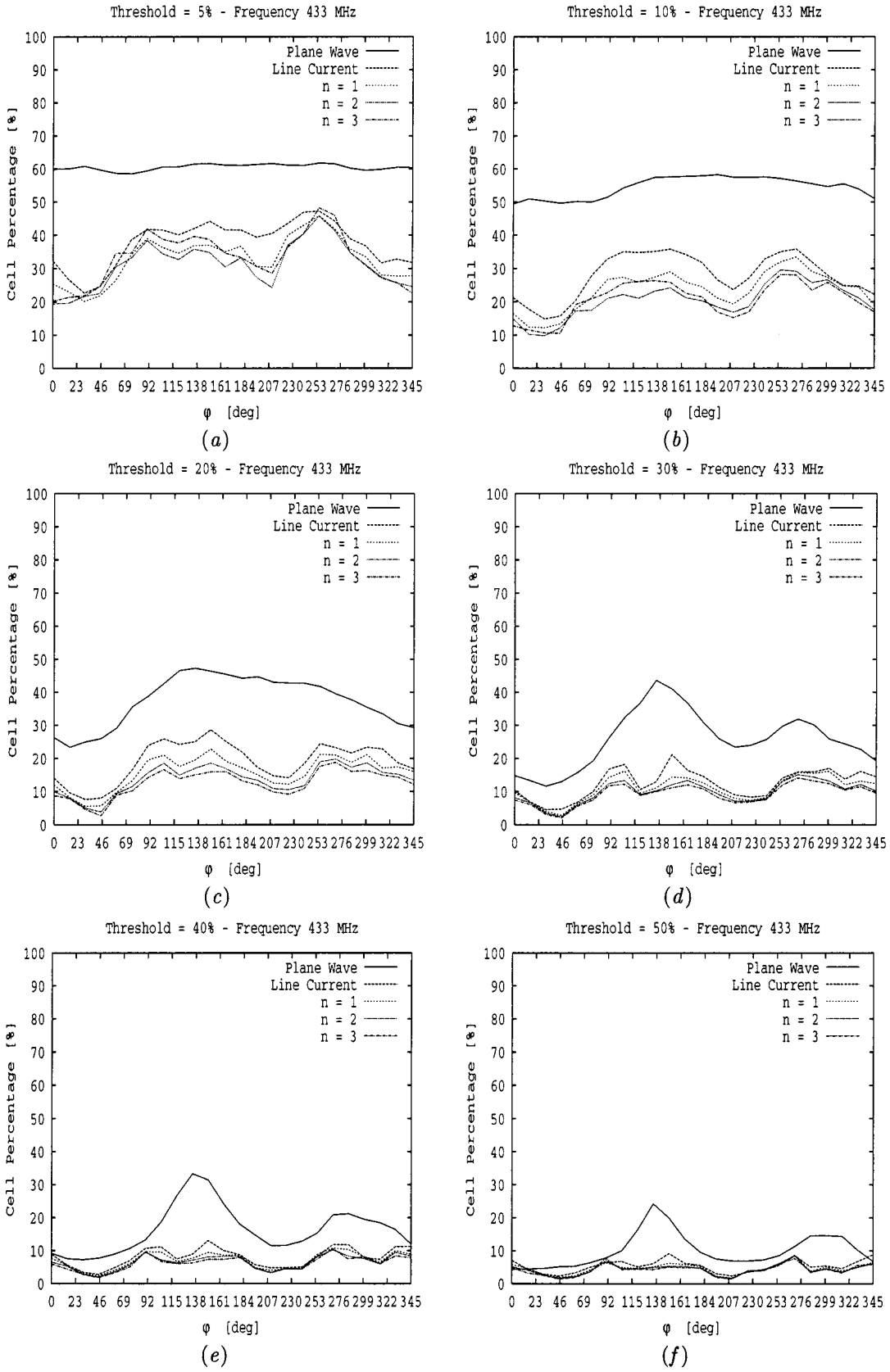

Fig. 2. Percentage of subdomains for which $|J_m| \geq J_{\rm th}$ (fixed threshold value) for the different considered illuminating sources. (a) $(J_{\rm th}/J_{\max}) = 5\%$. (b) $(J_{\rm th}/J_{\max}) = 10\%$. (c) $(J_{\rm th}/J_{\max}) = 20\%$. (d) $(J_{\rm th}/J_{\max}) = 30\%$. (e) $(J_{\rm th}/J_{\max}) = 40\%$. (f) $(J_{\rm th}/J_{\max}) = 50\%$. $J_{\max} = \max_m\{|J(x_m, y_m)|\}$.

R1 due to the presence of R2, whereas $\beta(\theta)$ is the total scattering contribution of R2. As can be deduced from Figs. 6 and 7, around $\theta = \pi$, the moderately focused source corresponding to $n = 2$ seems to be the better choice for imaging purposes as

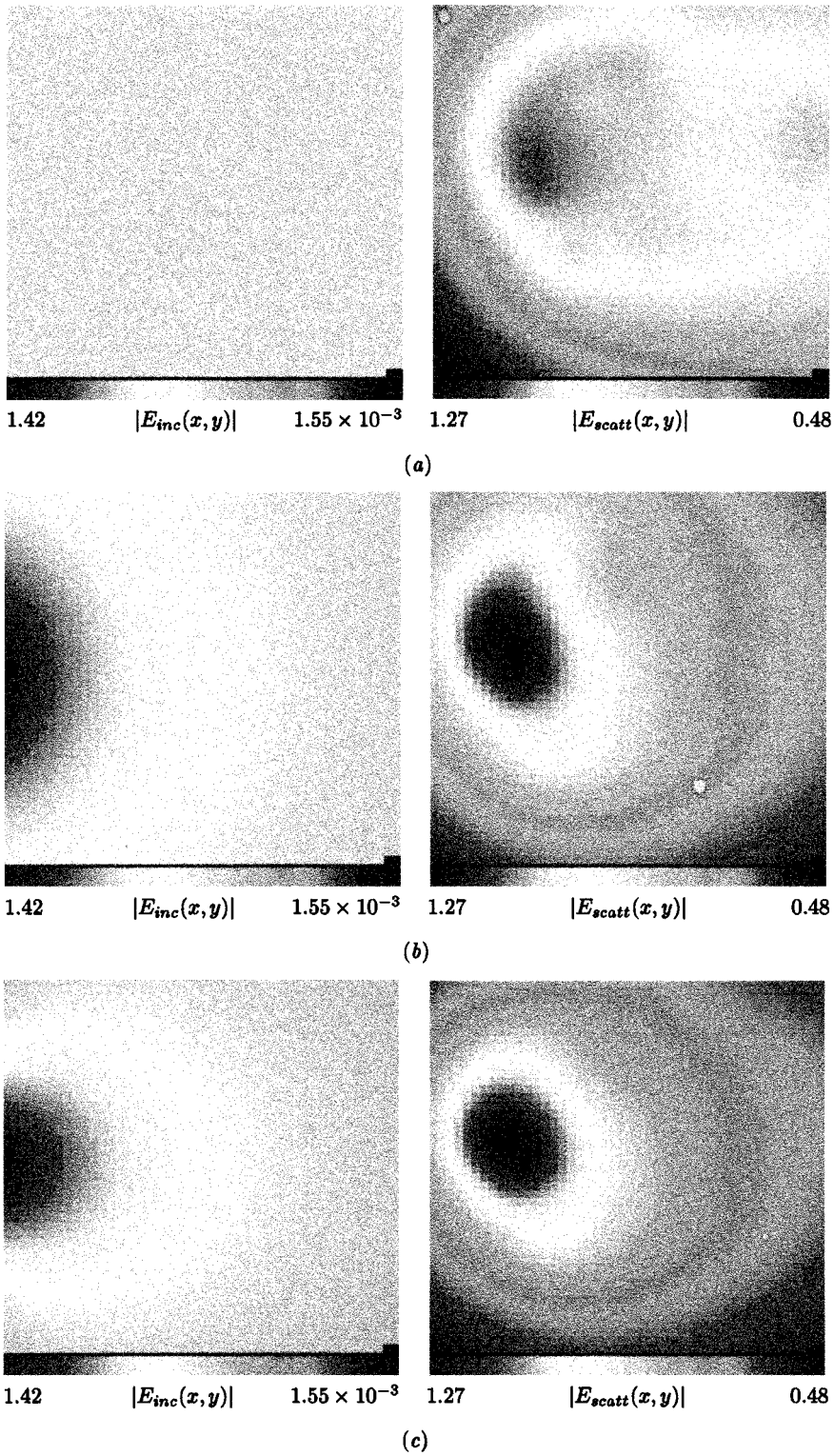

Fig. 3. Amplitude distributions of the incident and scattered electric fields inside the whole cross-sectional DI for different illuminating sources. Source position: $\varphi = \pi$. (a) Plane wave. (b) Infinite line current. (c) Focused source ($n = 1$).

both $\alpha(\theta)$ and $\beta(\theta)$ are very small. Of course, the plane-wave illumination results in large changes in the scattered field and the $\beta(\theta)$ term largely dominate.

The same computation has been performed by using higher frequency equal to 2.45 GHz although the used discretization is rather coarse at this frequency. As expected, the percentage of subdomains for which the related polarization current is greater than the fixed threshold results much smaller than the corresponding one in Fig. 2. In particular, a factor approximately equal to 1/2 has been found. For example, the percentage is less than 10% for $J_{\text{th}} \geq 10\%$ for all the positions of the source and for all sources excluding the plane-wave illumination (to save

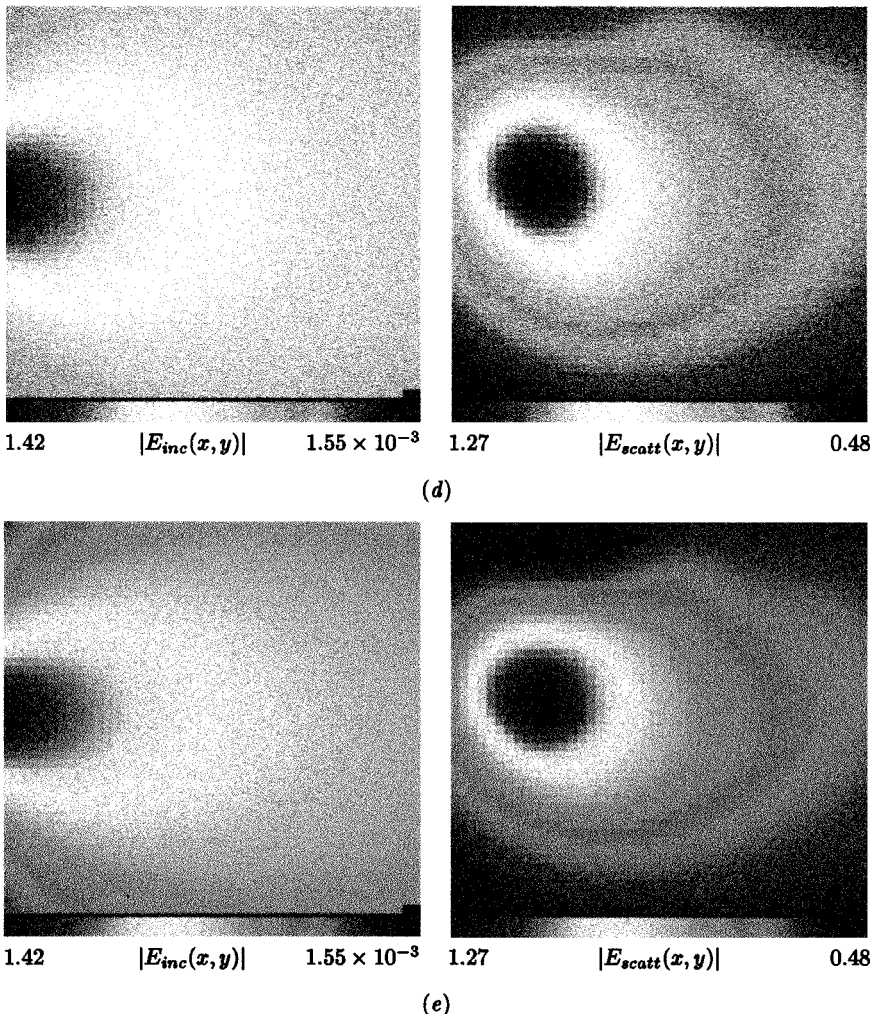

Fig. 3. *(Continued.)* Amplitude distributions of the incident and scattered electric fields inside the whole cross-sectional DI for different illuminating sources. Source position: $\varphi = \pi$. (d) Focused source ($n = 2$). (e) Focused source ($n = 3$). $f = 433$ MHz.

space, not all the plots are provided for this simulation). Certainly, this is related to the reduced penetration depth (e.g., in the liver, the penetration depth is about 0.71 cm at 2.45 GHz and about 2.6 cm at 433 MHz) that concentrates the scattering sources in the external layers of the biological bodies (as an example, Fig. 8 shows the distributions of the scattered electric field inside the investigation domain for the line current and the directive source corresponding to $n = 3$). In Fig. 9, the incident and scattered amplitudes for the same sources and along the x- and y-axes are also given. Although large parts of R1 and DI do not contribute significantly to the scattered field in DM, the fixed investigation domain is not very suitable at this frequency, as it could be deduced from Fig. 10, which should be compared with Fig. 7. Due to the stronger reflection at the external boundaries, large changes occur in the scattered field. Among those considered in this paper, the source with $n = 3$ seems to be better for this frequency.

We now consider the case in which the investigation domain moves at deeper positions inside the body. The possibility to investigate an internal portion of the body would be very important in medical application. It is obviously expected that the differences in the scattered data increase as the distance between the domain and external surface of the body increases. To quantitatively evaluate the weights of all the contributions involved in the computation of the scattered electric field, the following relative errors have been defined:

$$\gamma_1(\theta) = \frac{||E_{\text{scatt}}(b,\,\theta)| - |L_{11}(b,\,\theta) + L_{21}(b,\,\theta)||}{|E_{\text{scatt}}(b,\,\theta)|}$$

$$\gamma_2(\theta) = \frac{\alpha(\theta)}{|E_{\text{scatt}}(b,\,\theta)|}$$

and

$$\gamma_3(\theta) = \frac{\beta(\theta)}{|E_{\text{scatt}}(b,\,\theta)|}.$$

Fig. 11 gives the maximum, minimum, and average valued for each of the above normalized parameters and the related variance for different position inside the original cross-sectional DI at $f = 433$ MHz. The position of R1 is defined by its center, which is given by $(\rho_\ell,\,\pi)$. In particular, the position number ℓ in Fig. 11 is related to ρ_ℓ by the following relation: $\rho_\ell = s - (\ell - 1)\delta$ being $s = 8$ cm and $\delta = 1$ cm. As can be seen, from positions 1

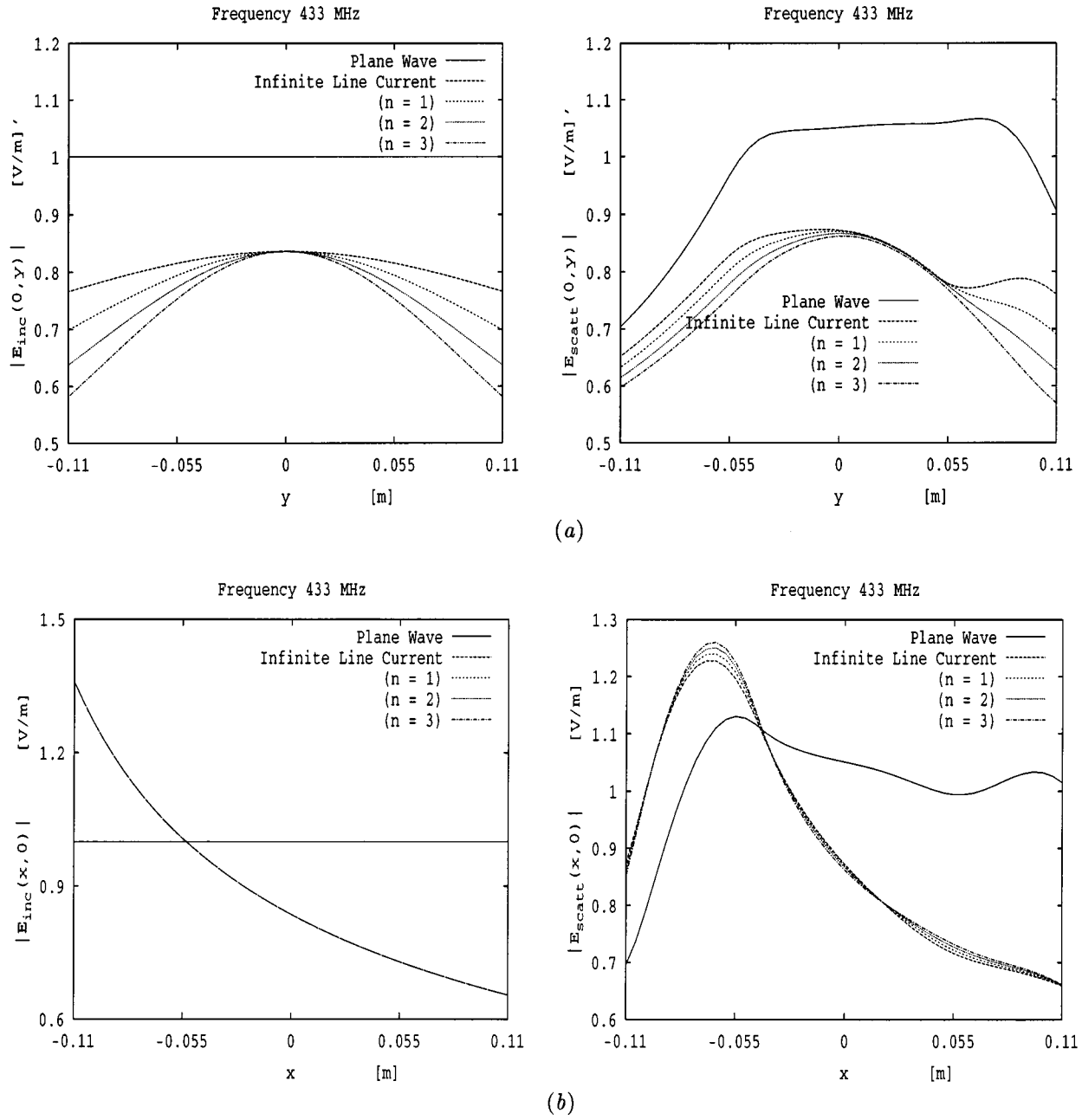

Fig. 4. Amplitude distributions of the incident and scattered electric fields for different illuminating sources along the: (a) vertical and (b) horizontal axes. $f = 433$ MHz.

to 7, γ_1 (the relative error on the scattered electric field in DM) slowly increases [see the average values in Fig. 11(c)] from less than 10% to about 30% (in this range, $\gamma_1(\theta)$ is almost constant for the plane-wave illumination). From positions 7 to 10, the error sharply increases (to about 50%) and becomes almost constant for deeper positions. The plots of $\gamma_2(\theta)$ and $\gamma_3(\theta)$ provide the behavior of the specific contributions to the scattering. From Fig. 11(m), it results that $\beta(\theta)$ can be neglected only for a few positions of R1.

At $f = 2.45$ GHz, the growing of all the plots is more regular and sharper. As an example, the average values of $\gamma_1(\theta)$, $\gamma_2(\theta)$, and $\gamma_3(\theta)$ are provided in Fig. 12. As can be seen, at the position $\ell = 2$, $\beta(\theta)$ cannot be neglected, whereas $\alpha(\theta)$ does not represent a significant contribution for $\ell \geq 7$.

III. Optimization Approach

Once the reduced domain has been defined, an optimization inverse method can be applied. As mentioned in Section I, in the authors' opinion, the use of an optimization approach is justified by several considerations. First of all, these methods are potentially able to reach the global minimum, avoiding false solutions ("artefacts"). This feature seems to be of great importance in medical applications, where it is very difficult (even from a psychological point-of-view) to accept to use a diagnostic tool that does not ensure (even in principle) that the "right" solution can be obtained.

The approach used here is based on a GA, which has been previously developed in [29] (Born approximation) and [30],

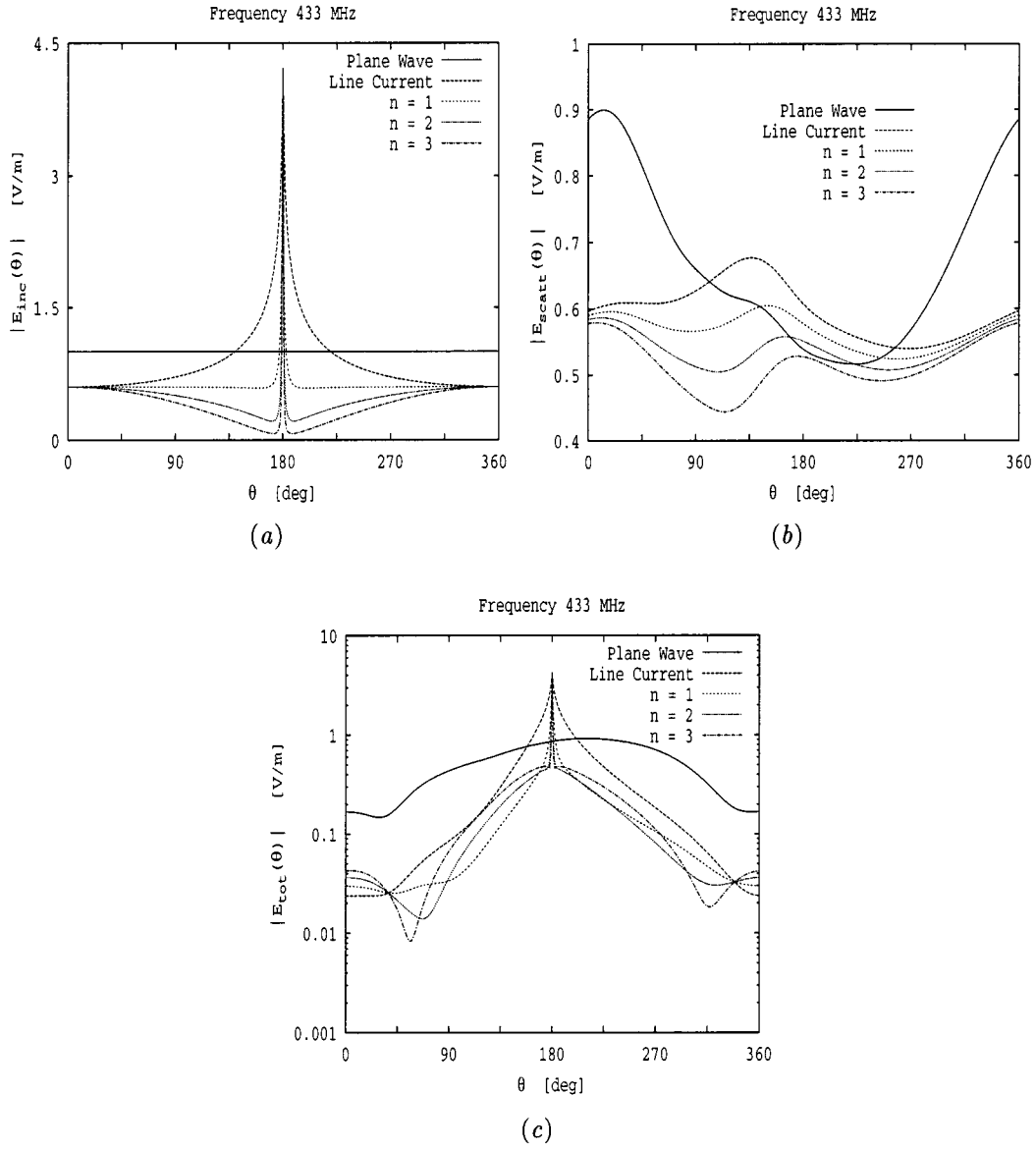

Fig. 5. Amplitudes of the: (a) incident, (b) scattered, and (c) total electric fields at the measurement points of the observation domain DM (radius $b = 16.4$ cm) for different illuminating sources. Source position: $\varphi = \pi$.

[31], but not yet applied in biomedical areas. In short, the GA is an iterative approach aimed at minimizing a functional that, in the present medical application, can be defined as

$$U\left\{\tau_1^*(x, y), E_{\mathrm{tot}_1}^*(x, y)\right\} = a_1 \left| \sum_{p=1}^{P} \left\{ E_{\mathrm{scatt}}(b, \theta_p) - L_e(b, \theta_p) \right\} \right|^2 + a_2 \left| \sum_{m=1}^{N_1} \left\{ E_{\mathrm{inc}}(x_m, y_m) - \left[E_{\mathrm{tot}}^*(x_m, y_m) - L_o(x_m, y_m) \right] \right\} \right|^2 \quad (3)$$

where L is given by

$$L(x, y) = \sum_{k=1}^{N_1} \tau_k^* E_{\mathrm{tot}_k}^* G_k(x, y)\, \Delta \quad (4)$$

where $G_k(x, y)$ is the integral of the Green function calculated on the kth subdomain (whose area is Δ), the subscript o refers the case in which $(x, y) \in \mathrm{R1}$, and the subscript e, the case in which $(x, y) \in \mathrm{DM}$ (observation domain). In equation (3), N_1 is the number of subdomains of R1, P is the number of measurement points, and a_1 and a_2 are two regularization constants to be fixed. This functional is constituted by two terms, sometimes called "data" and "state" terms, respectively. Other terms can be added (e.g., penalty terms), but this subject is beyond the scope of this paper. The asterisk indicates quantities that are now unknown.

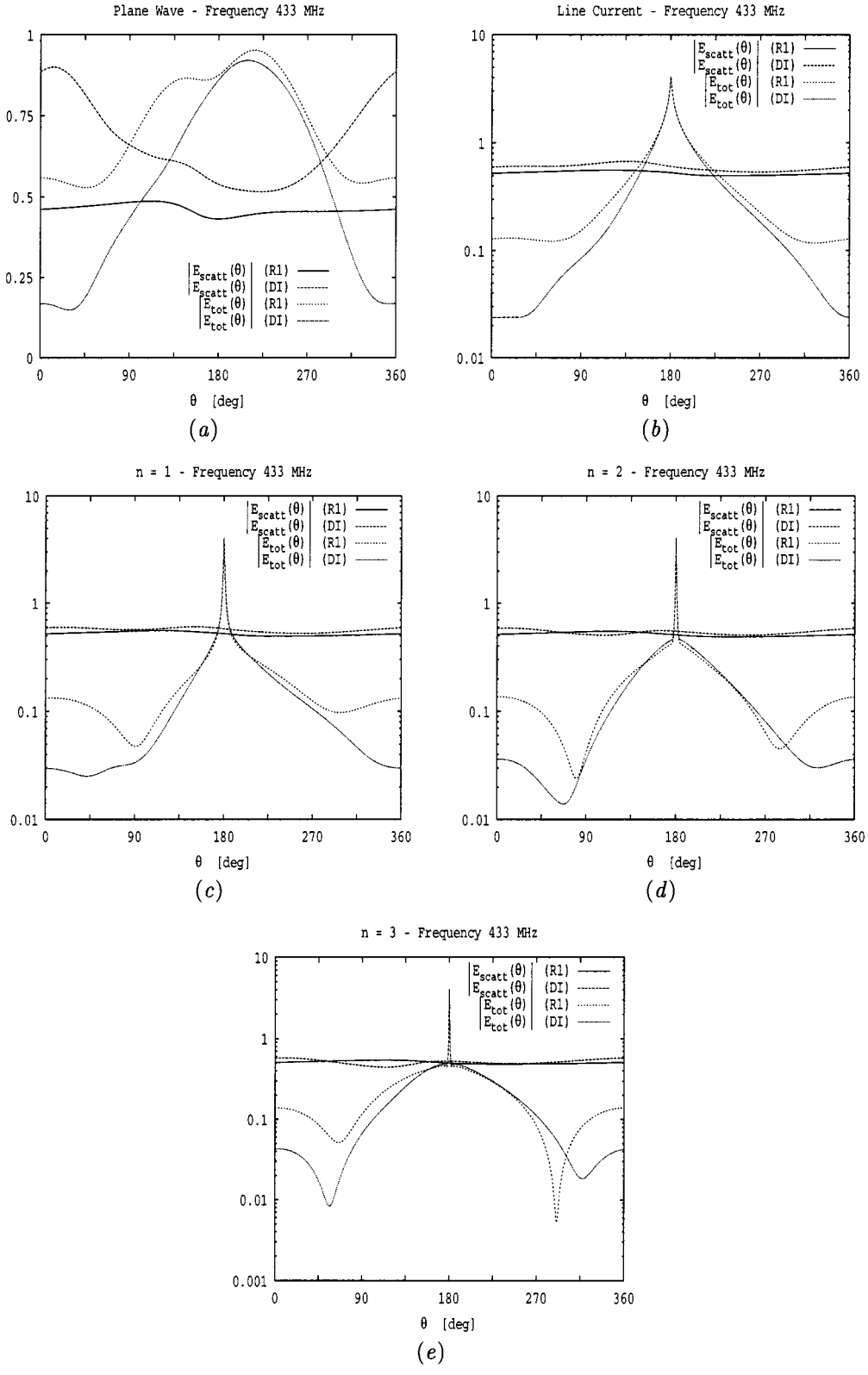

Fig. 6. Comparisons between the case in which only the reduced investigation domain R1 (side $d = 7.5$ cm) is considered and the case in which the whole cross-sectional DI is assumed. Amplitudes of the scattered and total electric fields in the observation domain DM. Source position: $\varphi = \pi$. (a) Plane wave. (b) Infinite line current. (c) Focused source ($n = 1$). (d) Focused source ($n = 2$). (e) Focused source ($n = 3$).

The minimization of the functional is performed by applying a GA, which is based on a random search of the (global) minimum. The approach requires an *initialization* phase, where a set of M trial solutions is randomly generated and constitutes a *population of chromosomes*. At this point, the iterative process starts and the population at a generic step $k + 1$ is computed

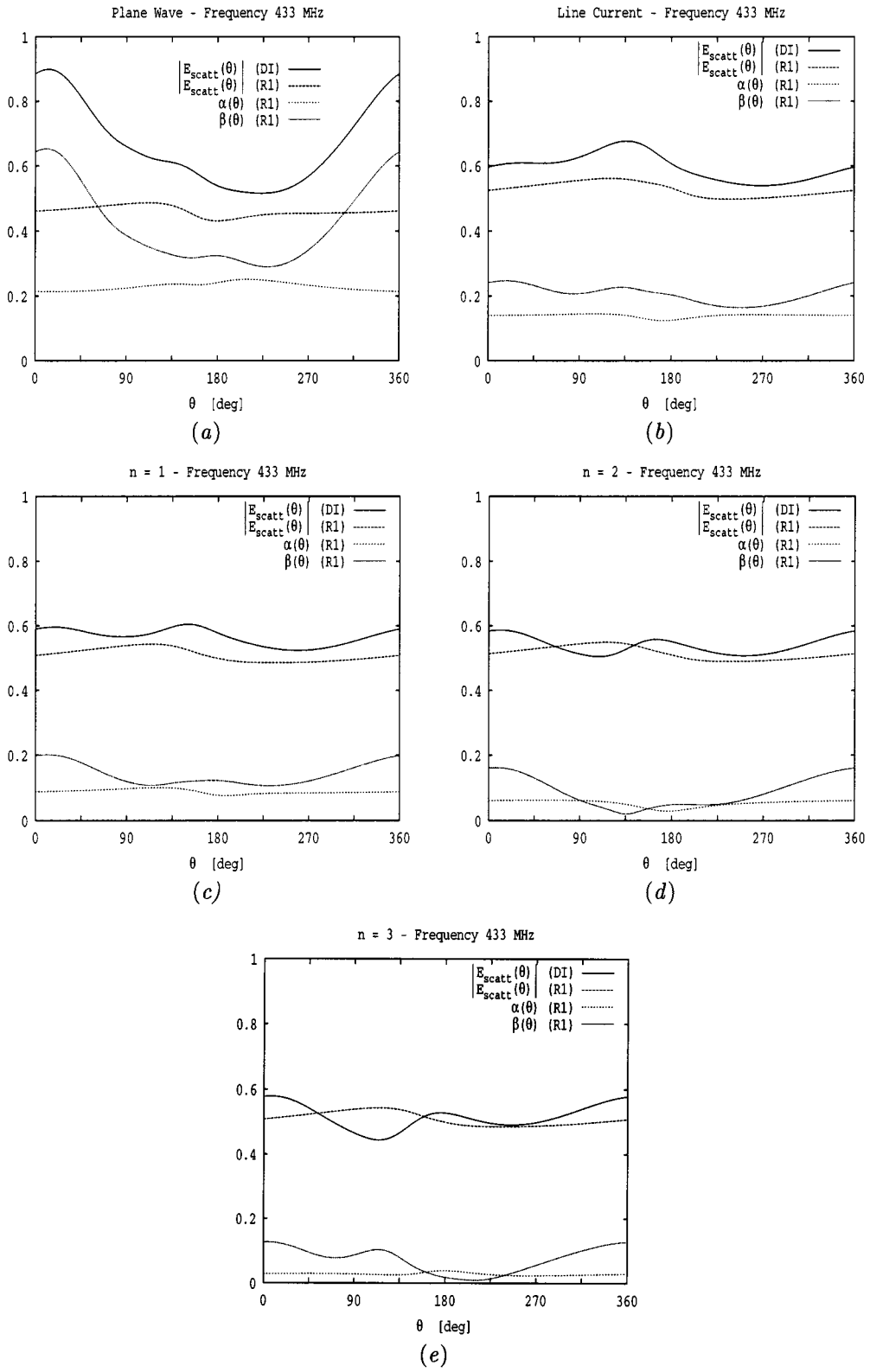

Fig. 7. Plots of the contributions to the scattered electric field denoted by $\alpha(\theta)$ and $\beta(\theta)$ [see (1)]. Scattered and total electric fields (amplitudes). (a) Plane wave. (b) Infinite line current.

on the basis of the population at step k by using the genetic operators of selection, crossover, and mutation [21]–[23]. The iterative process continues until a stopping criterion is satisfied ($U^{(k)} \leq U_{\rm th}$, $U_{\rm th}$ being a fixed threshold) or a given number of iterations is completed. For the simulations performed in this paper, the following parameters have been used, according to open literature on the subject [22], [23] and on the basis of some previously obtained results in imaging of inhomogeneous two-dimensional scatterers, mainly in the light of nondestructive testing applications. In particular, $M = 100$ (population

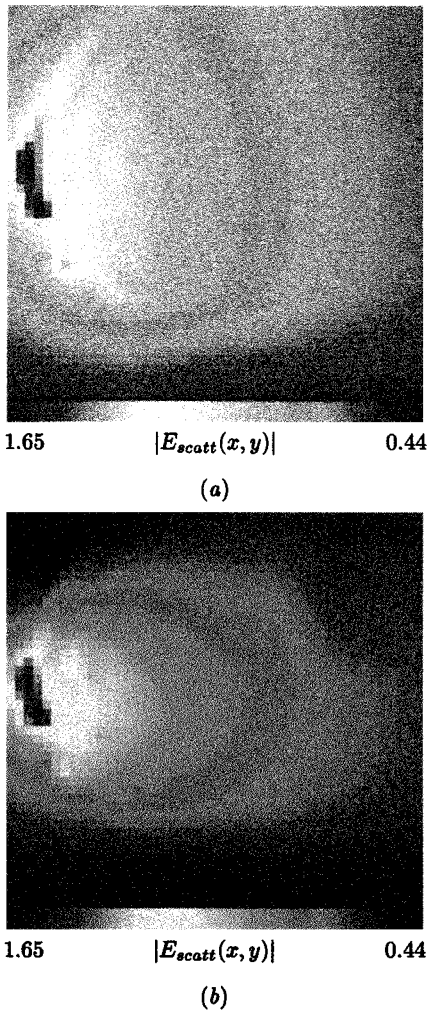

Fig. 8. Amplitude distributions of the scattered electric field inside DI. Source position: $\varphi = \pi$. (a) Infinite line current. (b) Focused source ($n = 3$). $f = 2.45$ GHz.

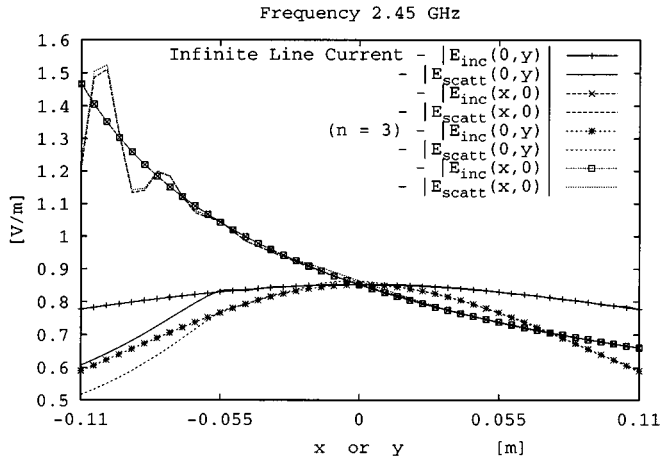

Fig. 9. Amplitude distributions of the incident and scattered electric fields for the infinite line current and focused source ($n = 3$) sources along the x- and y-axes. $f = 2.45$ GHz.

dimension), $P_{\text{cross}} = 0.7$ (crossover probability), $P_{\text{mut}} = 0.8$ (mutation probability), $U_{\text{th}} = 10^{-3}$, $a_1 = 10.0$, and $a_2 = 1.0$. The equally spaced $P = 225$ measurement points have angular

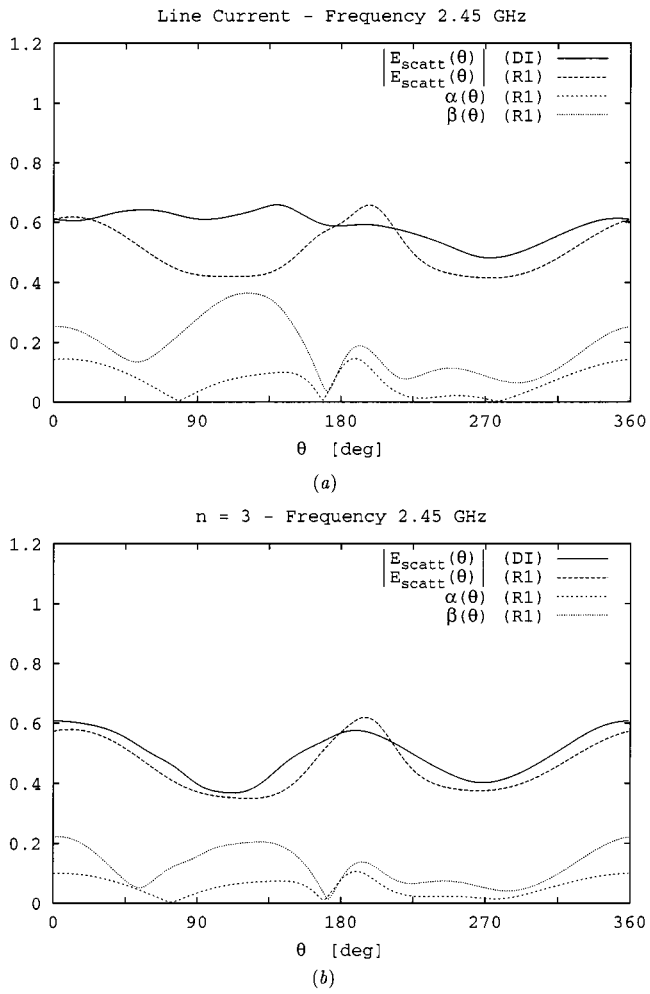

Fig. 10. Plots of the contributions to the scattered electric field denoted by $\alpha(\theta)$ and $\beta(\theta)$ [see (1)]. Scattered and total electric fields (amplitudes). (a) Infinite line current. (b) Focused source ($n = 3$). $f = 2.45$ GHz.

coordinates in the range $163^\circ \leq \varphi \leq 197^\circ$ and synthetic data are used as input data. In the initialization phase, the field unknowns are randomly chosen by means of a random uniform distribution of values in the range

$$\left\{ \min_{(x,y)\in \text{DI}} [-2|\text{Re}(E_{\text{inc}}(x,y))|]; \max_{(x,y)\in \text{DI}} [2|\text{Re}(E_{\text{inc}}(x,y))|] \right\}$$

for the real part and in the range

$$\left\{ \min_{(x,y)\in \text{DI}} [-2|\text{Im}(E_{\text{inc}}(x,y))|]; \max_{(x,y)\in \text{DI}} [2|\text{Im}(E_{\text{inc}}(x,y))|] \right\}$$

for the imaginary part. The starting values for the object function are randomly selected between $0 + j0$ and

$$2\left(\max_{(x,y)\in \text{DI}} \{\text{Re}[\tau_{\text{ref}}(x,y)]\} + j \max_{(x,y)\in \text{DI}} \{\text{Im}[\tau_{\text{ref}}(x,y)]\} \right)$$

where τ_{ref} indicates the actual distribution.

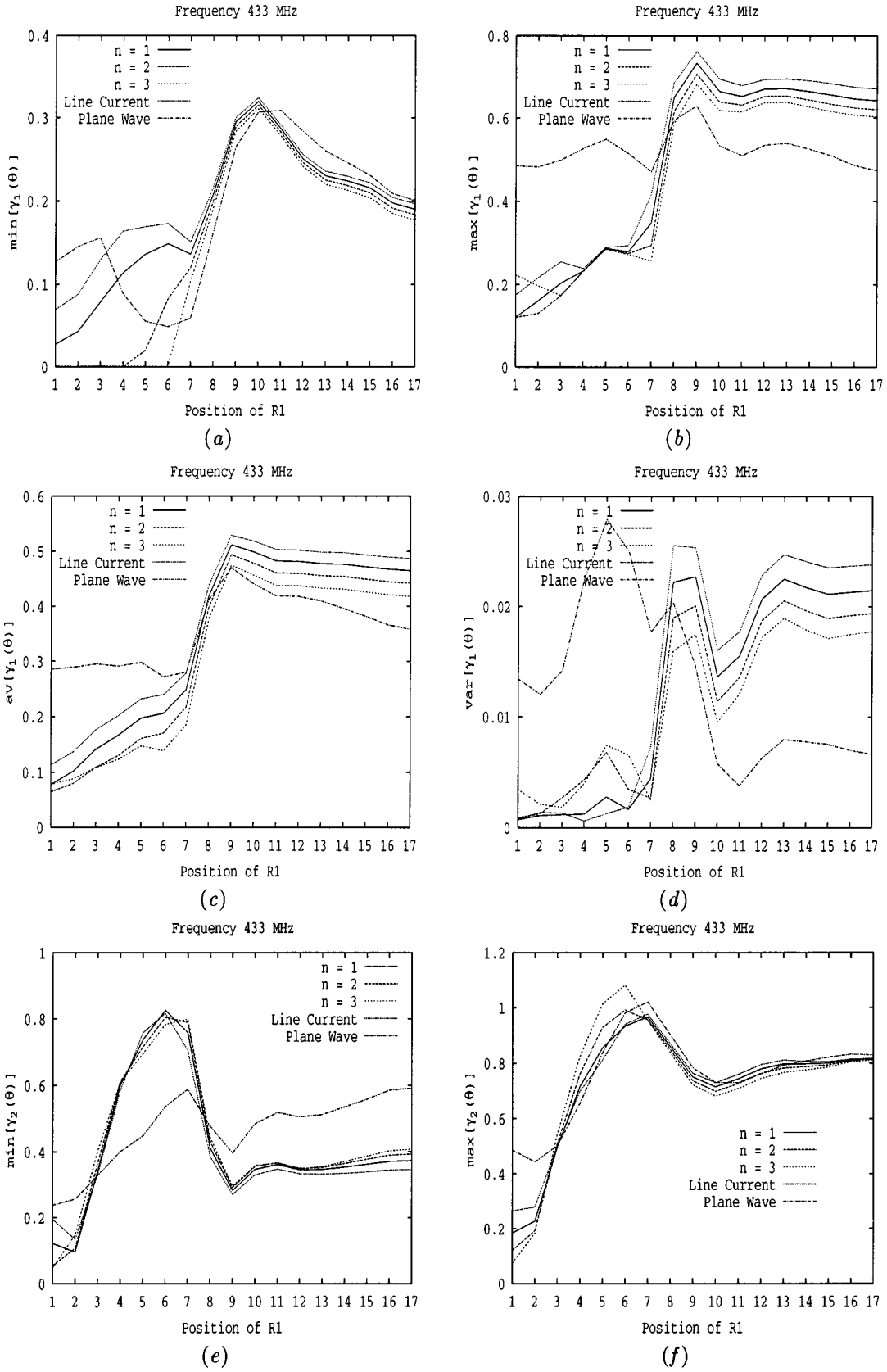

Fig. 11. Behavior of the quantitative parameters $\gamma_1(\theta)$, $\gamma_2(\theta)$, and $\gamma_3(\theta)$ for different positions of the reduced investigation domain inside the abdomen and for different illuminating sources. (a), (e) Minimum. (b), (f), Average. (c) Maximum values (with respect to the polar angle θ). (d) Variance distributions. $f = 433$ MHz.

Fig. 13 shows the original and reconstructed images of R1. Although no additional penalty terms are used and no *a priori* information is considered, in the reconstruction of the real part of the scattering potential (related to the relative dielectric per-

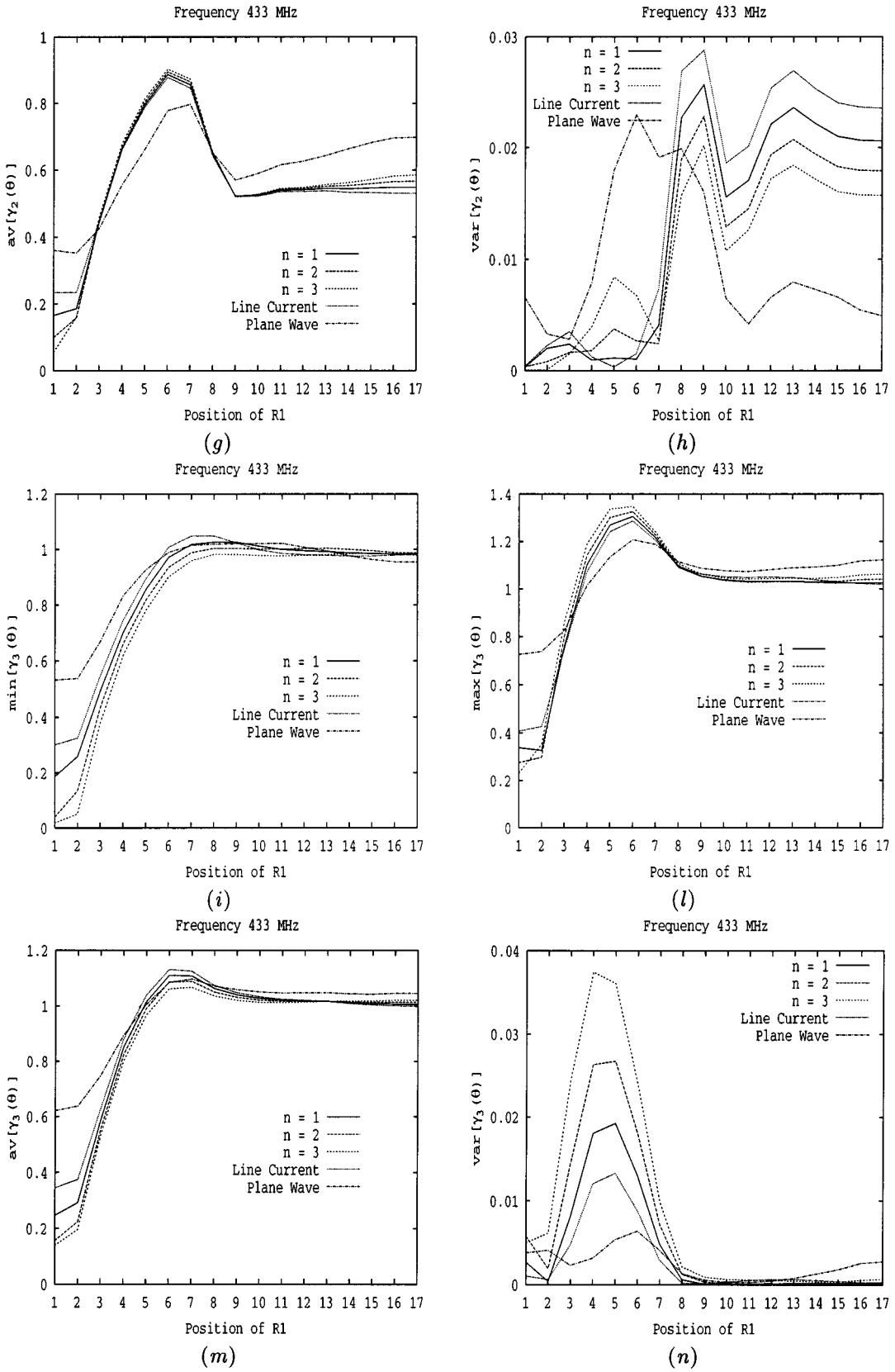

Fig. 11. *(Continued.)* Behavior of the quantitative parameters $\gamma_1(\theta)$, $\gamma_2(\theta)$, and $\gamma_3(\theta)$ for different positions of the reduced investigation domain inside the abdomen and for different illuminating sources. (g), (m) Maximum values (with respect to the polar angle θ). (h), (n) Variance distributions. $f = 433$ MHz. (i) Minimum. (l) Average.

mittivity), the boundaries between different tissues are rather accurately located and, more importantly, the obtained values are close to the original ones (this demonstrate the feasibility of a quantitative imaging). On the contrary, significant errors are

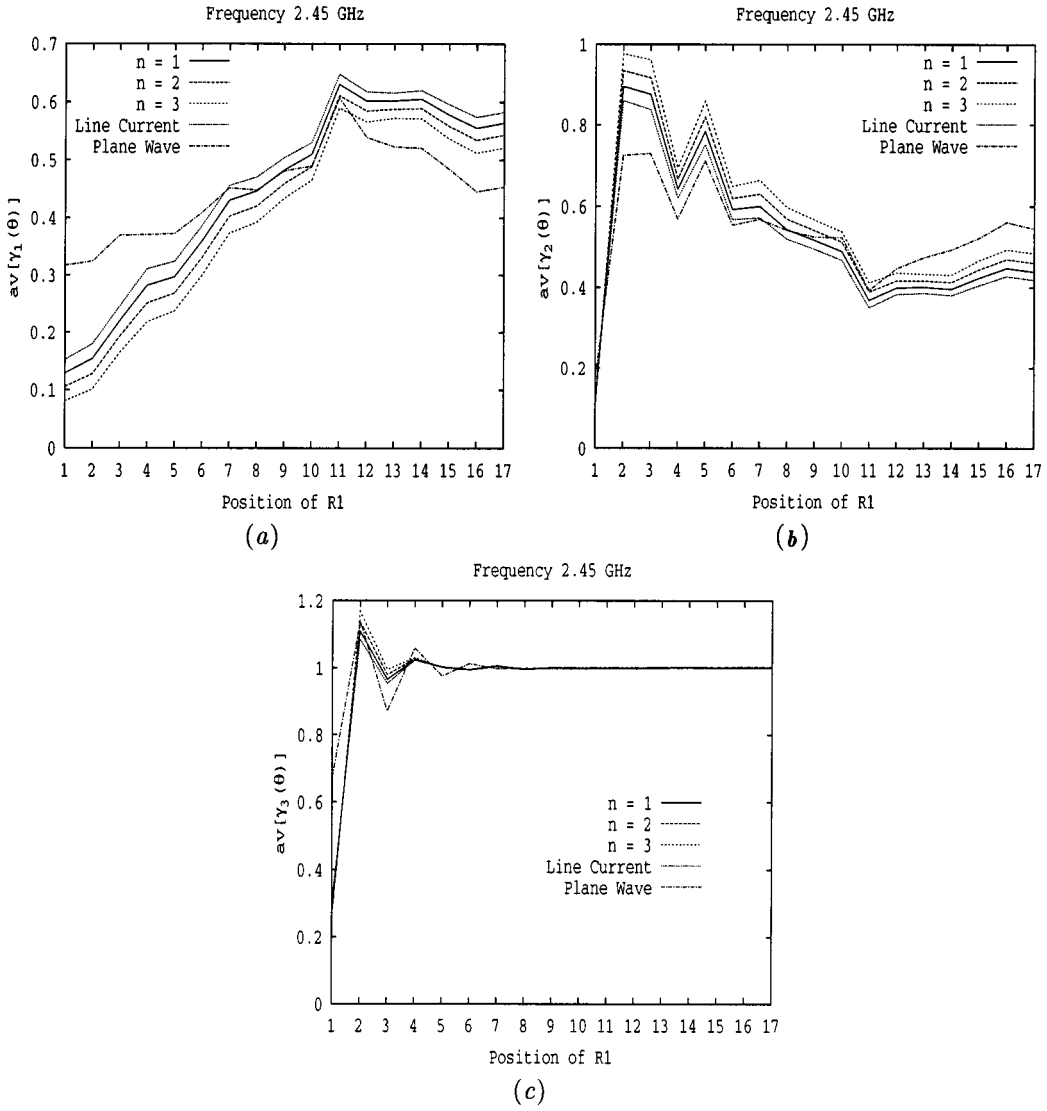

Fig. 12. Behavior of the average values of: (a) $\gamma_1(\theta)$, (b) $\gamma_2(\theta)$, and (c) $\gamma_3(\theta)$ for different positions of the reduced investigation domain inside the abdomen and for different illuminating sources. $f = 2.45$ GHz.

present in the reconstruction of the imaginary part (related to the electric conductivity). Although it is generally recognized that the reconstruction of the electric conductivity is more critical, it should be noted that these reconstruction have been obtained by using a single view process. Better results should be obtained if multiillumination/multiview conditions were used.

IV. Conclusions

The possible application of a global optimization technique based on a GA to imaging biological bodies exposed to interrogating microwaves has been evaluated by means of numerical forward simulations. For the text case considered (a human abdomen), it has been shown that a reduced investigation domain can be used with limited errors on the measured scattered data. The possibility of reducing the investigation domain seems to be related to the use of moderately focusing sources. Once the domain has been selected (on the basis of the polarization current density, which is responsible for the scattering contribution of each part of the scatterer), the global optimization technique can be applied. In the medical field, the possibility of using a method, which allows, in principle, to reach the global minimum and allows the insertion of a lot of *a priori* information, is, in the authors' opinion, very appealing. Moreover, the approach allows to use information drawn from different diagnostic tools, as the data can be inserted both as continuous and discrete quantities (e.g., information about boundaries between adjacent tissues). Since the main emphasis of this paper was on the numerical assessment related to the possible reduction of the investigation domain, the imaging capabilities of the inverse approach should be further checked with reference to models relevant in the medical field. From a methodological point-of-view, the GA, when applied to the inversion of simple and canonical dielectric scatterers, has been already tested in [29]–[31], mainly with reference to nondestructive-testing purposes. For example, the possibility of considering only certain specific values of the dielectric parameters, corresponding to biological tissues (or small ranges of values centered around this discrete values), will be

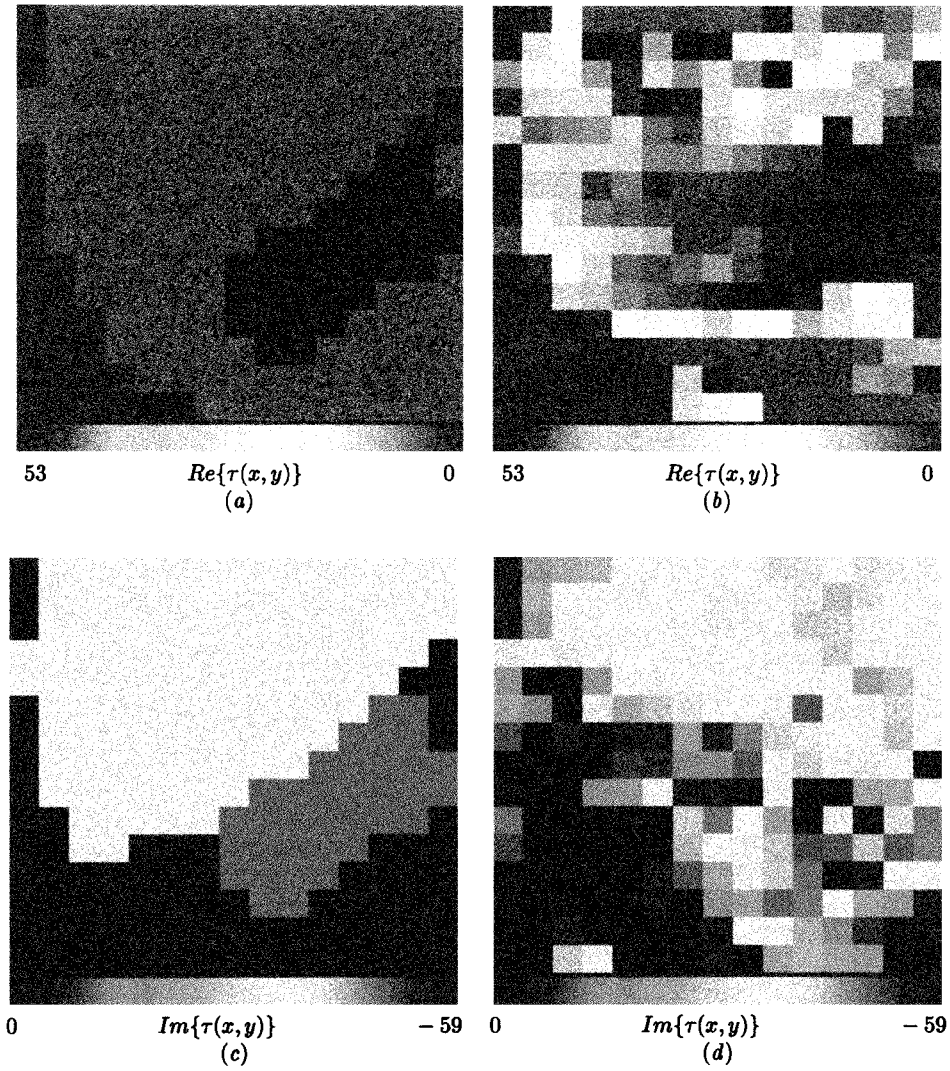

Fig. 13. Reconstructed distribution of the scattering potential inside the reduced investigation domain R1 ($d = 7.5$ cm) at position $l = 1$. Real part: (a) original, (b) reconstructed. Imaginary part: (c) original, (d) reconstructed. $f = 433$ MHz.

the subject of a future investigation. This assumption should greatly increase the speed of the GA (at present, about 5-h CPU time are necessary on a PC). In addition, assuming as known the boundaries among different organs (obtained by standard medical imaging tools) should provide a dramatic simplification of the approach. The two above developments are very difficult to be implemented if deterministic inversion approaches are used. Finally, with some care, the GA can be used in conjunction with deterministic methods (e.g., gradient methods). The study of the application of this hybrid technique to imaging inhomogeneous dielectric has been started and we hope it can represent a further development in microwave imaging for medical diagnostics. In conclusion, the authors of this paper believe that microwave imaging can still be considered a diagnostic technique with potential advantages over more consolidated methods (as it was considered in several pioneering works, some which were mentioned in Section I). Nevertheless, the study and definition of specific application conditions should be pursued since a straightforward application of existing inversion methodologies (at least to whole biological systems) seems to be rather difficult and not very effective when considering the present levels of imaging technology and computer power.

REFERENCES

[1] L. E. Larsen and J. H. Jacobi, Eds., *Medical Applications of Microwave Imaging*. New York: IEEE Press, 1986.

[2] M. Vanden-Bossche and A. Barel, "Necessity of simulation tools in parameter identification problems concerning image," in *Proc. 2nd European Simulation Congr.*, Ghent, Belgium, 1986, pp. 601–605.

[3] C. Pichot, L. Jofre, G. Perronet, and J. C. Bolomey, "Active microwave imaging of inhomogeneous bodies," *IEEE Trans. Antennas Propagat.*, vol. AP-33, pp. 416–425, Apr. 1985.

[4] T. Nakajima, H. Sawada, and I. Yamaura, "Microwave CT imaging for a human forearm at 3 GHz," *IEICE Trans. Commun.*, vol. E78-B, no. 6, pp. 874–882, 1995.

[5] B. Yazgan, S. Paker, and M. Kartal, "Image reconstruction with diffraction tomography using different inverse radon transform algorithms," in *Proc. Int. Biomed. Eng.*, Istanbul, Turkey, Aug. 18–20, 1992.

[6] A. Broquetas, J. Romeu, J. M. Rius, A. R. Elias-Fusté, A. Cardama, and L. Jofre, "Cylindrical geometry: a further step in active microwave imaging," *IEEE Trans. Microwave Theory Tech.*, vol. 39, pp. 836–844, May 1991.

[7] M. J. Hagmann and R. L. Levine, "Procedures for noninvasive electromagnetic property and dosimetry measurements," *IEEE Trans. Antennas Propagat.*, vol. 38, pp. 99–106, Jan. 1990.
[8] D. K. Ghodgaonkar, O. P. Gandhi, and M. J. Hagmann, "Estimation of complex permittivities of three-dimensional inhomogeneous biological bodies," *IEEE Trans. Microwave Theory Tech.*, vol. MTT-31, pp. 442–446, June 1983.
[9] P. M. Meaney, K. D. Paulsen, J. T. Chang, M. W. Fanning, and A. Hartov, "Nonactive antenna compensation for fixed-array microwave imaging: Part II—Imaging," *IEEE Trans. Med. Imag.*, vol. 18, pp. 508–518, Jun. 1999.
[10] A. Vander Vorst, "Microwave bioelectromagnetics in Europe," in *Proc. IEEE MTT-S Microwave Symp. Dig.*, Atlanta, GA, June 1993, pp. 1137–1140.
[11] T. C. Guo and W. W. Guo, "3-D dielectric imaging by inverse scattering with resolution unlimited by wavelength," in *Annu. Rep. Elect. Insulation Dielectric Phenomena Conf.*, Leesburg, VA, 1989, IEEE Paper 89CH2773-0, pp. 65–74.
[12] S. Caorsi, G. L. Gragnani, M. Pastorino, and M. Rebagliati, "A model-driven approach to microwave diagnostics in biomedical applications," *IEEE Trans. Microwave Theory Tech. (Special Issue)*, vol. 44, pp. 1910–1920, Oct. 1996.
[13] J. J. Mallorquí and A. Broquetas, "Microwave inverse scattering: biomedical and industrial applications," in *Proc. Progress in Electromag. Res. Symp.*, Seattle, WA, 1995, p. 330.
[14] C. Pichot, P. Lobel, L. Blanc-Féraud, M. Barlaud, K. Belkebir, J. M. Elissalt, and J. M. Geffrin, "Gradient and Newton–Kantorovich methods for microwave tomography," in *Inverse Problems in Medical Imaging and Nondestructive Testing*, H. W. Engl, A. K. Louis, and W. Rundell, Eds. Berlin, Germany: Springer-Verlag, 1997, pp. 168–187.
[15] S. Caorsi, G. L. Gragnani, S. Medicina, M. Pastorino, and G. A. Pinto, "A Gibbs random field-based active electromagnetic method for noninvasive diagnostics in biomedical applications," *Radio Sci.*, vol. 30, pp. 291–301, 1995.
[16] W. C. Chew and Y. M. Wang, "Reconstruction of two-dimensional permittivity distribution using the distorted Born iterative method," *IEEE Trans. Med. Imag.*, vol. 9, pp. 218–225, June 1990.
[17] R. E. Kleinman and P. M. van den Berg, "Two-dimensional location and shape reconstruction," *Radio Sci.*, vol. 29, p. 1157, 1994.
[18] A. Broquetas, J. J. Mallorquí, J. M. Rius, L. Jofre, and A. Cardama, "Active microwave sensing of highly contrasted dielectric bodies," *J. Electromag. Wave Applicat.*, vol. 7, pp. 1439–1453, 1993.
[19] M. Bertero and P. Boccacci, *Introduction to Inverse Problems in Imaging*. Bristol, U.K.: IOP Press, 1998.
[20] M. Slaney, A. C. Kak, and L. E. Larsen, "Limitation of imaging with first-order diffraction tomography," *IEEE Trans. Microwave Theory Tech.*, vol. MTT-32, pp. 860–873, Aug. 1984.
[21] D. E. Goldberg, *Genetic Algorithms in Search, Optimization, and Machine Learning*. Reading, MA: Addison-Wesley, 1989.
[22] R. L. Haupt, "An introduction to genetic algorithms for electromagnetics," *IEEE Antennas Propagat. Mag.*, vol. 37, pp. 7–15, Feb. 1995.
[23] D. S. Weile and E. Michielssen, "Genetic algorithm optimization applied to electromagnetics: A review," *IEEE Trans. Antennas Propagat*, vol. 45, pp. 343–353, Mar. 1997.
[24] M. Pastorino, "Short-range microwave inverse scattering techniques for image reconstruction and applications," *IEEE Trans. Instrum. Meas.*, vol. 47, pp. 1419–1427, Dec. 1998.
[25] R. F. Harrington, *Field Computation by Moment Method*. New York: Macmillan, 1968.
[26] M. Ney, "Method of moments as applied to electromagnetic problems," *IEEE Trans. Microwave Theory Tech.*, vol. MTT-33, pp. 972–980, Oct. 1985.
[27] C. A. Balanis, *Antenna Theory: Analysis and Design*. New York: Wiley, 1997.
[28] K. R. Foster and H. P. Schwan, "Dielectric properties of tissues," in *Handbook of Biological Effects of Electromagnetic Fields*, C. Polk and E. Postow, Eds. Boca Raton, FL: CRC Press, 1986.
[29] S. Caorsi and M. Pastorino, "Two-dimensional microwave imaging approach based on a genetic algorithm," *IEEE Trans. Antennas Propagat.*, to be published.
[30] S. Caorsi, A. Massa, and M. Pastorino, "Nonlinear inverse scattering approach for image reconstruction by using a genetic algorithm," in *Proc. Int. Nonlinear Electromag. Syst. Symp.*, Pavia, Italy, May 10–12, 1999, p. 153.
[31] S. Caorsi and M. Pastorino, "Microwave nondestructive testing: A stochastic optimization approach," in *Electromagnetic Nondestructive Evaluation (II)*. ser. Studies in Applied Electromagnetics and Mechanics, D. Lesselier and A. Razek, Eds. Amsterdam, The Netherlands: IOS Press, 1999, vol. 15, pp. 145–156.

Salvatore Caorsi (M'98) is currently a Full Professor of electromagnetic compatibility in the Department of Electronics, University of Pavia, Pavia, Italy. He also teaches a course on antennas at the University of Genoa, Genoa, Italy. He is the Past-President and Founding Member of the Inter-University Research Center for Interactions Between Electromagnetic Fields and Biological Systems (ICEMB). His primary activities are focused on applications of electromagnetic fields to telecommunications, artificial vision and remote sensing, biology, medicine, and electromagnetic compatibility.

Prof. Caorsi is a member of the Associated Electrical Industries (AEI), European Bioelectromagnetic Association (EBEA), and the European Society for Hyperthermic Oncology (ESHO).

Andrea Massa received the Laurea degree in electronic engineering and Ph.D. degree in electronics and computer science from the University of Genoa, Genoa, Italy, in 1992 and 1996, respectively.

He is currently an Assistant Professor of electromagnetic fields in the Department of Biophysical and Electronic Engineering, University of Genoa, where he also teaches the "Electromagnetic Fields 1" course. He is a member of the Inter-University Research Center for Interactions Between Electromagnetic Fields and Biological Systems (ICEMB). Since 1992, his research work has been principally concerned with electromagnetic direct and inverse scattering, wave propagation in the presence of nonlinear media and chiral media, and applications of electromagnetic fields to telecommunications, medicine, and biology.

Matteo Pastorino (M'90–SM'96) is currently an Associate Professor of electromagnetic fields in the Department of Biophysical and Electronic Engineering, University of Genoa, Genoa, Italy, where he is responsible for the Applied Electromagnetics Group, and currently teaches the "Electromagnetic Fields and Remote Sensing and Electromagnetic Diagnostics" course. His main research interests are in the field of electromagnetic direct and inverse scattering, microwave imaging, wave propagation in presence of nonlinear media, and analytical and numerical methods in electromagnetism.

Dr. Pastorino is a member of the IEEE Instrumentation and Measurement Technical Committee on Imaging Systems. He is also a member of the Associazione Elettrotecnica ed Elettronica Italiana (AEI) and the European Bioelectromagnetic Association (EBEA).